Article

Structural, Optical and Photocatalytic Properties of Aluminium Scrap from End – of – Life Vehicles Modified TiO2 Nanoparticle

Ramona – Crina Suciu *, Simona Elena Avram *, Andreia Molea, Codruta Varodi, Cristian Tudoran, Maria Stefan, Adriana Popa, Dana Toloman

Posted Date: 4 December 2023

doi: 10.20944/preprints202312.0192.v1

Keywords: Aluminiu scrap; end – of – life vehicles; composite material; photocatalysis

Article

Structural, Optical and Photocatalytic Properties of Aluminium Scrap from End – of – Life Vehicles Modified TiO_2 Nanoparticle

Ramona-Crina Suciu [1,*], Simona Elena Avram [2,*], Andreia Molea [3], Codruța Varodi [1], Cristian Tudoran [1], Maria Ștefan [1], Adriana Popa [1] and Dana Toloman [1]

[1] National Institute for Research and Development of Isotopic and Molecular Technologies, Donat Street, No. 67-103, 400293 Cluj-Napoca, Romania
[2] Faculty of Materials and Environmental Engineering, Technical University of Cluj-Napoca, 103-105 Muncii Bd., 400641 Cluj-Napoca, Romania
[3] Department of Automotive and Transport Engineering, Technical University of Cluj-Napoca, 103-105 Muncii Bd., 400641 Cluj-Napoca, Romania
* Correspondence: Ramona.Suciu@itim-cj.ro (R.-C.S.); simona.avram@imadd.utcluj.ro (S.E.A.)

Abstract: The recycling of wastes to obtain value-added products is a great challenge in the sustainable economy. In our studies, a mixed precursor containing aluminium scrap from end – of – life vehicles and TiO_2 Degussa P25 was used to prepare TiO_2 modified Al photocatalyst through solid state reaction. Al scrap and TiO_2 Degussa P25 in the ration of n(Ti) / n(Al) = x (x = 0.0 - 2.5), and acetylacetonate and Tween 80 was mixed under magnetic stirring and sintered using a conventional furnance at 550°C. DTA – TG – DTG, X – ray diffraction, Fourier – transform infrared, UV – Vis and photoluminescence spectroscopies were assed to investigate the thermal, structural, optical properties and photocatalytic activity. The effect of aluminium concentration on the characteristics of TiO_2 Degussa P25 depending on the above instruments are studied. XRD revealed that the materials have crystal structure of anatase TiO_2, rutile TiO_2 and aluminium. The opto-electronic properties show that Al addition shifted the absorption spectra toward the visible range. The photocatalytic performance of Al – TiO_2 composites was quantified by the degradation of Allura Red solution under a visible condition. The highest photocatalytic activity (79.99%) was achieved for the sample containing 0.5% Al and a higher concentration of Al particles shields the active centres of the semiconductor, thus reducing its photocatalytic activity. Aluminium scrap from end-of-life vehicles can be a source of raw material to be considered in semiconductor production. The spin-trapping technique evidenced that $\bullet O^{2-}$ was the main species generated responsible for the Allura Red degradation.

Keywords: Aluminiu scrap; end – of – life vehicles; composite material; photocatalysis

1. Introduction

End-of-life vehicles (ELVs) have become an emerging challenge associated with the rapid growth in the world economy and industrial development because of their large and increasing production volumes. Aluminium alloys are widely used in the automotive and aerospace industries due to their high specific strength and corrosive resistance. Because this alloys can no more satisfy the increasing requirements of the market, aluminium – matrix composite materials reinforced with solid particles, have attracted extensive attention, becoming more extensive studied [1–3] and aluminium scrap (old and new) [4–7] become the most widely recycled non-ferrous metals in the world [3,8,9].

End-of-life vehicles (ELVs) have become an emerging challenge associated with the rapid growth in the world economy and industrial development because of their large and increasing production volumes. Aluminium alloys are widely used in the automotive and aerospace industries due to their high specific strength and corrosive resistance. Because this alloys can no more satisfy the increasing requirements of the market, aluminium – matrix composite materials reinforced with

Preprints (www.preprints.org) | NOT PEER-REVIEWED | Posted: 4 December 2023 doi:10.20944/preprints202312.0192.v1

solid particles, have attracted extensive attention, becoming more extensive studied [1,2,10] and aluminium scrap (old and new) [11–14] become the most widely recycled non-ferrous metals in the world [3,15,16].

2. Results

2.1. Precursor solution analysis

2.1.1. Thermal analysis

The thermal analysis TG–DTA–DTG was performed on the dried at room temperature, for 10 days and heat treated at 150°C for 2h on 2.5%Al doped titanium precursor's solution in the temperature range 20 – 1000°C at a heating rate of 10°C/min in an airflow (Figure 1) in order to establish the optimum crystallization temperature for the corresponding oxides. From the TGA curves weight loss is in majority characterized by two different zones. First, weight loss falling in the range 0 – 350°C due to moisture removal, decomposition of amorphous carbon from Tween 80 and acetylacetone. The second zone in the range 350 – 1000°C is due to several structural changes, such as conversion of the anatase phase of TiO_2 in rutile, aluminium melting.

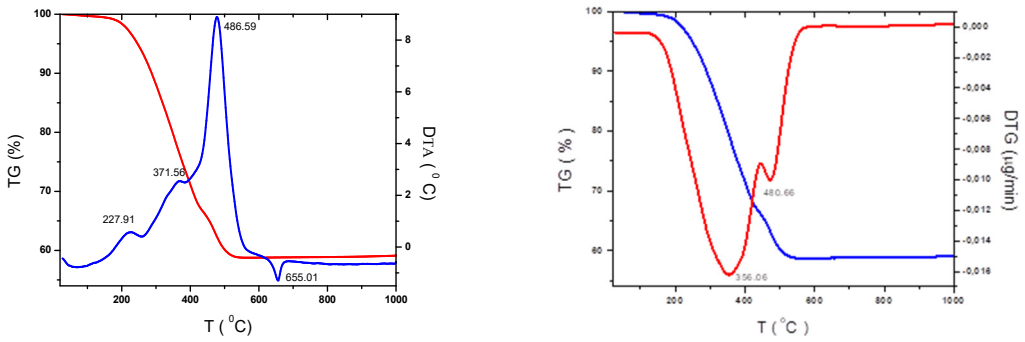

(**a**) (**b**)

Figure 1. The TG–DTA–DTG curves thermogram of the dried (150°C) titania precursors.

2. 2 Nanopowder solution analysis

2.2.1. X–ray diffraction analysis

The XRD patterns of TiO_2 Degussa P25 and Al - TiO_2 composites after calcination at 500°C for 2h, are shown in Figure 2. XRD diffraction patterns illustrate the fact that all titania samples contain the tetragonal anatase crystalline phase (PDF card 00-021-1272), rutile (PDf card 01-076-0318) and Al (PDF card 00-004-0787). The presence of this phases in the materials indicate the absence of a chemical reduction mechanism [17]. The absence of other peaks, specially of Al_2O_3 thin film which can be formed on surface due to easily oxidation of Al, means that formed alumina on the Al surface is non-crystalline [18].

The Lee at el. [19] observed reduction of grain size and presence a lower crystallinity weaking intensity of the anatase (101) peak with increasing de Al contents, confirmed by Rietveld rafination.

Preprints (www.preprints.org) | NOT PEER-REVIEWED | Posted: 4 December 2023 doi:10.20944/preprints202312.0192.v1

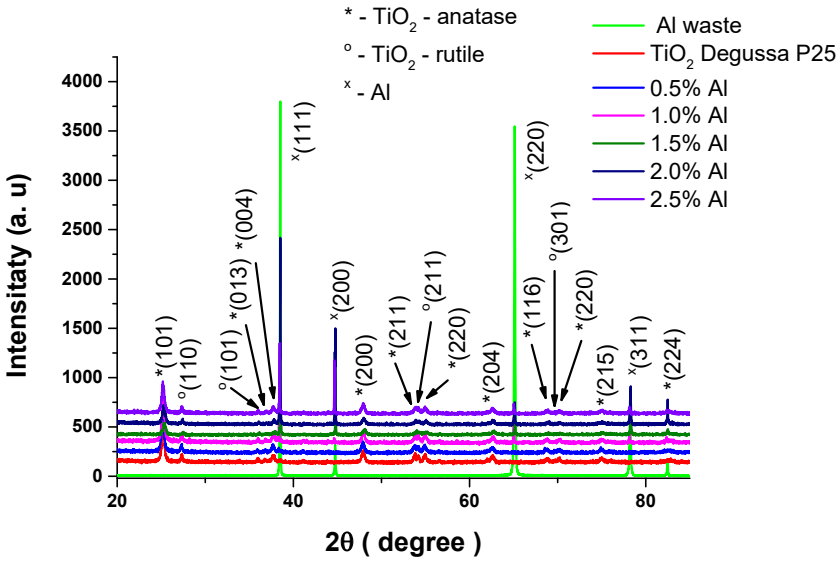

Figure 2. XRD patterns of Al - TiO_2 nanoparticles.

In order to determine the effective crystallite mean size (D_{eff}) the Warren - Averbach X-ray profile Fourier analysis of the (101) (2θ = 25.209°), (004) (2θ = 37.527) and (200) (2θ = 47.874°) anatase peak profiles were processed by the XRLINE [20] computer program. The crystallite size distribution function was determined from the second derivative of the strain corrected Fourier coefficients [21].

By single X-ray profile Fourier analysis of Ag - TiO_2 nanoparticles, the microstructural information such as the effective crystallite mean size, D_{eff} (nm), the root mean square (rms) of the microstrains averaged along the real space distance, $\langle \varepsilon^2 \rangle_{hkl}^{1/2}$ were obtained [22].

Rietveld type refinement for determination of elementary parameters of the cell was performed with the Powder Cell program [25], developed by Werner Kraus & Gert Nolze (BAM Berlin).

The cell parameters of sample are close, due to the structural distortions that break the crystal continuity induced by Al^{3+} addition [26], but the a and c parameter change slightly, as results the cell volume changes. According with literature the influence of Al on the cell volume and unit cell are contradictory [27]: introduction of Al increase in the crystal lattice parameters a and c [28] or have opposite effect, depending on the sources of aluminium (salts, metallic aluminium …).

Table 1. The effective crystalline mean size, D_{eff} (nm), the root mean square (rms) of the microstrains averaged along the real space, $\langle \varepsilon^2 \rangle_{hkl}^{1/2}$.

Sample	Precent [%]			Unit cell parameter		Cell volume [Å³]	Effective crystalline mean size, D_{eff} (mm)	Microstrains averaged along the real space, $\langle \varepsilon^2 \rangle_{hkl}^{1/2} \times 10^3$
	Al	TiO_2 anatase	TiO_2 rutile	a [Å]	c [Å]			
TiO_2 Degussa P25	-	88.1	11.9	3. 8019	9.5353	137.83	24.805	7.54
0.5% Al	1.607	87.9	10.49	3.800	9.5346	137.67	24.72	7.69
1.0% Al	3.515	87.735	8.75	3.7935	9.5368	137.15	24.65	7.73
1.5% Al	5.241	87.21	7.54	3.7936	9.5268	137.10	24.51	7.82
2.0% Al	7.097	87.183	5.72	3.7838	9.5206	136.52	24.38	7.92
2.5% Al	9.12	86.76	4.12	3.7863	9.5122	136.36	24.22	8.03

Preprints (www.preprints.org) | NOT PEER-REVIEWED | Posted: 4 December 2023 doi:10.20944/preprints202312.0192.v1

2.2.2. FT – IR spectroscopy

FT – IR spectroscopy in the 4000 – 450cm^{-1} region (Figure 3) was carried out to estimate the variation in the functional groups, which influence the interface formed with the absorber layer and the electronic structure [27]. The vibrational mode peak present around 3000 to 3650cm^{-1} attributed to the hydroxy functional groups, which is present on the surface of TiO_2 and / or bonded to Al^{3+} [28]. The peak around 1600 cm^{-1} is associated with anatase phase or Me – O, Ti – O, and Ti – O – Me stretching vibration [27,29,30]. The broadband between 450-1000cm^{-1} is related to the stretching vibration of Ti – O – Ti [31].

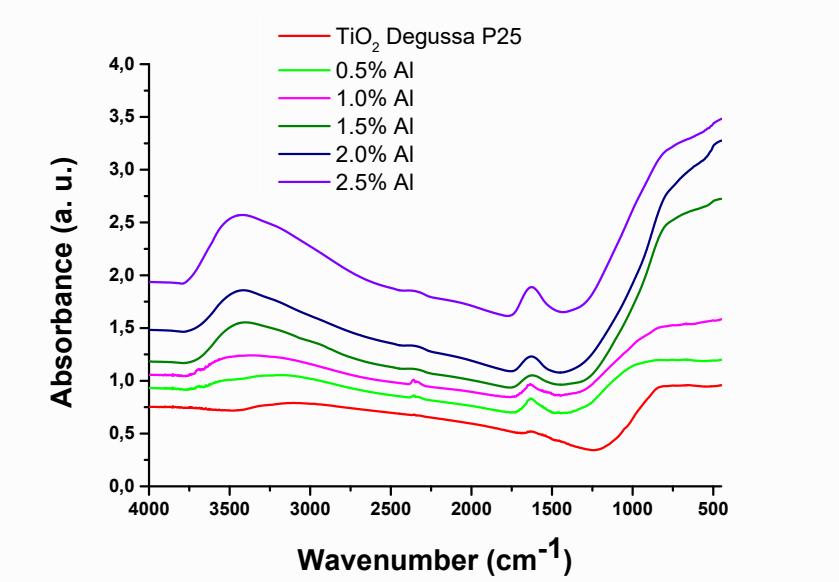

Figure 3. FT – IR spectra of Al – TiO_2 samples.

2.2.3. UV -Vis spectroscopy

Figure 4 reveals the infrared spectra of the samples. The absorption range of Al – TiO_2 samples shows a red shift compared with undoped TiO_2 due to Al incorporating into the titania framework and reduction of band – gap caused by the transition of sp electron of aluminium to the conduction band of TiO_2 [32].

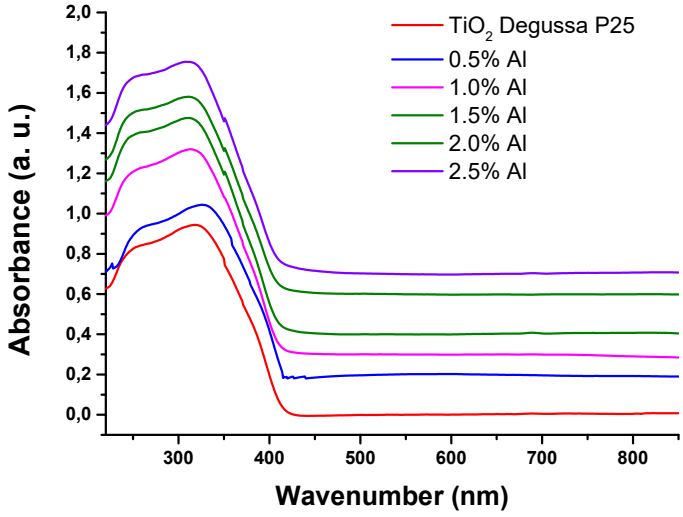

Figure 4. UV – VIS spectrum of Al modified TiO_2 nanoparticle.

Preprints (www.preprints.org) | NOT PEER-REVIEWED | Posted: 4 December 2023 doi:10.20944/preprints202312.0192.v1

2.2.4. Optical band gap energy, E_g determination

Based on the optical absorption edge obtained from the UV – Vis spectra, the energy band gaps (E_g) for the synthesized samples were estimated using the Tauc's equation by plotting $(Ahv)^n$, where A is the absorption coefficient, and $h\nu$ is the photon energy. The value of $n = \frac{1}{2}, \frac{3}{2}, 2$ *or* 3 depending on the nature of the electronic transition responsabile for absorption. Based on the obtained results that are given in Figure 5. The nedoped titania posses a band gap almost equal with the pure titania anatase $(E_g = 3.0 - 3.2eV)$ [33]. This difference is due to the presence in this case of two crystal structure: anatase and rutil, which broaden the range of the absorption for TiO_2 [34]. After de Al addition the indirect band gap *(n = 2)* is reduced from 2.98 to 2.82eV and for $n = \frac{1}{2}$ (direct band gap) is 2.99 to 2.81eV, respectively. The shift in the absorbance implies a reduction in the bandgap due to the narrowing of the bandgap energy by Al addition and formation of intermediates states between the valence bands and conduction bands [3,27,35,36].

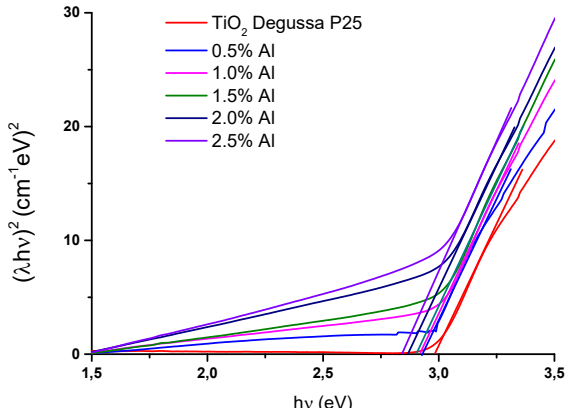

Figure 5. Extrapolation of the band gap energy for direct band gap.

2.2.5. Morphology of nanocomposites

The morphology of the as prepared samples is shown in Figure 6. The agglomeration was present due to strong van der Waals interaction, as was observed by Ray [37].

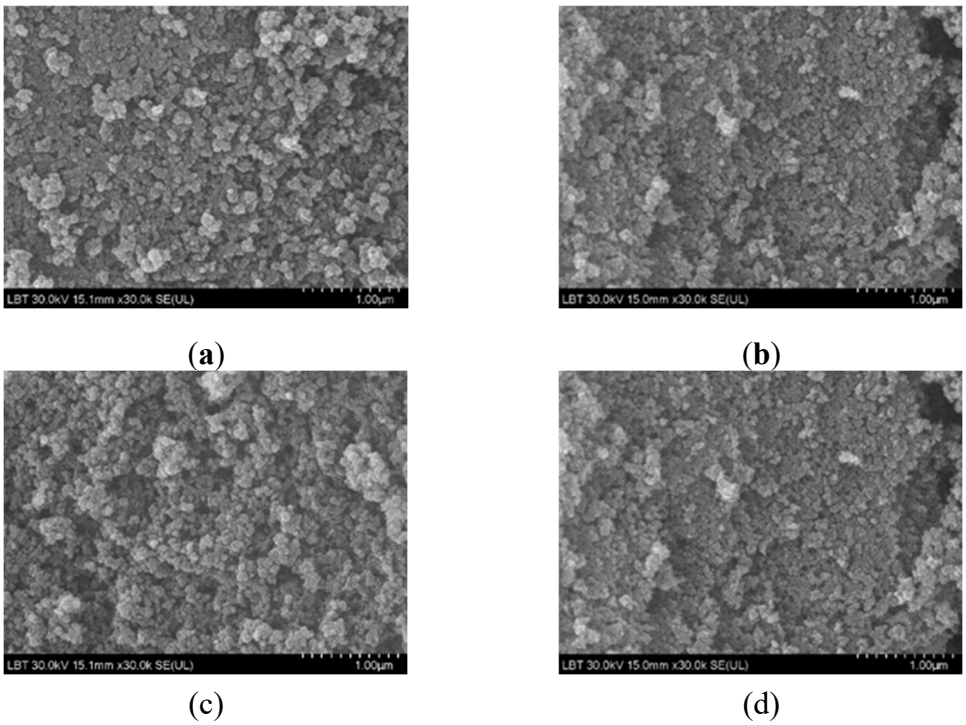

(a) **(b)**

(c) (d)

Preprints (www.preprints.org) | NOT PEER-REVIEWED | Posted: 4 December 2023 doi:10.20944/preprints202312.0192.v1

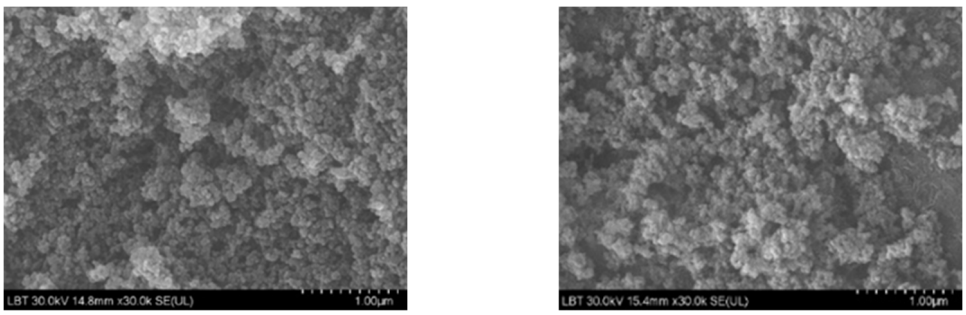

(e) (f)

Figure 6. Morfology of composites granule. (a) TiO_2 Degussa P25, (b) 0.5% Al, (c) 1.0% Al, (d) 1.5% Al, (e) 2.0% Al and (f) 2.5% Al.

The elemental composition of the 0 – 2.5% Al was determined through energy dispersive X-rays analysis (EDX, Figure 7). EDX analysis revealed that amount of introduced aluminium varied in the range 2.8 to 28.2 wt% for all samples (Table 2).

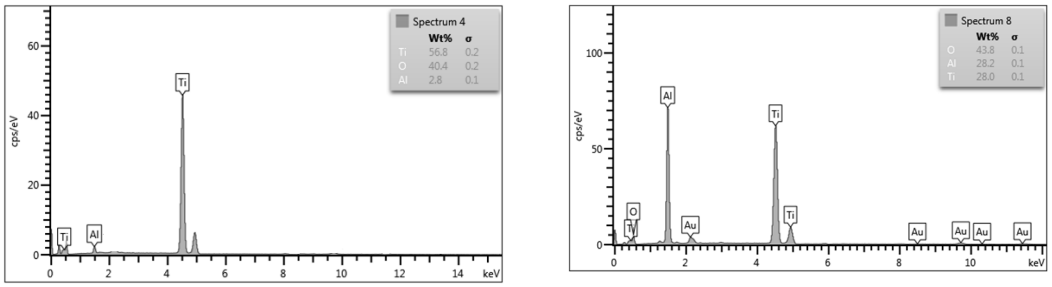

(a) **(b)**

Figure 7. EDX spectra of the Al modified TiO_2 nanoparticle. (a) 0.5% Al and (b) 2.5% Al.

Table 2. Atomic percentage of Al modified TiO_2 nanoparticles as prepared samples corresponding to EDX examinations.

Sample	Mass ratio (%)		
	O	Ti	Al
Al waste	47.1	-	52.9
TiO2 Degussa P25	40	60	-
0.5% Al	40.4	56.8	2.8
1.0% Al	41.2	48.2	10..6
1.5% Al	42.5	45.9	13.4
2.0% Al	43	35.2	21.9
2.5% Al	43.8	28.0	28.2

2.2.6. Photoluminescence spectroscopy

The PL spectra of Al – TiO_2 nanoparticle with different amount of Al particles is illustrated in Figure 8. The emission band at 378nm is attributed to band – to – band excitation [38,39]. Emission around ~465nm is related to defect stress formed by oxygen vacancies [ ] and defect levels below the conduction band of titania nanoparticles [40] and blue-green emission at 485nm can be attribute the charge transfer from Ti^{3+} to oxygen anion in a $[TiO_6]^{8-}$complex associated with oxygen vacancies at the surface. This presence is originating from the intrinsic state rather the surface state [41].

Additional peaks at 510 nm belongs to oxygen vacancies on the surface of titania nanoparticles [42].

Preprints (www.preprints.org) | NOT PEER-REVIEWED | Posted: 4 December 2023 doi:10.20944/preprints202312.0192.v1

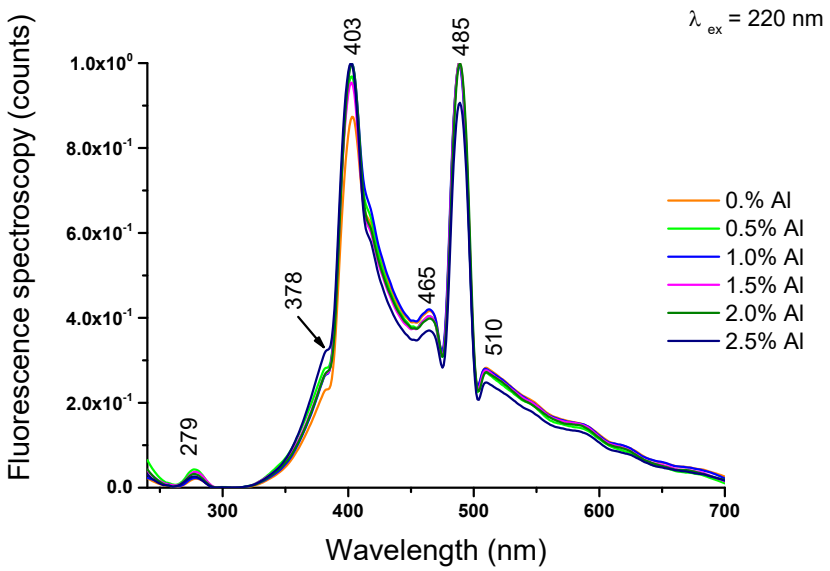

Figure 8. Photoluminescence spectra of Al - TiO_2 nanomaterials.

2.2.7. Photocatalytic activity determination

In order to evaluate the photocatalytic activity of the Al modified TiO_2 nanoparticles, the degradation of Allura Red in aqueous solution was carried out at room temperature under UV irradiation (365nm). To obtain a good dispersion and ensure absorption – desorption equilibrium, the solution was stirred for 1h in a dark position inside the photo-reactor before light irradiation.

The efficiency of the photocatalysts for selected Allura Red degradation was calculated according to equation: $F\ (\%) = \frac{C_o - C_t}{C_0}\ x\ 100$, where c_o is the initial dye concentration and C_t is the concentration of dye at time t (Figure 9).

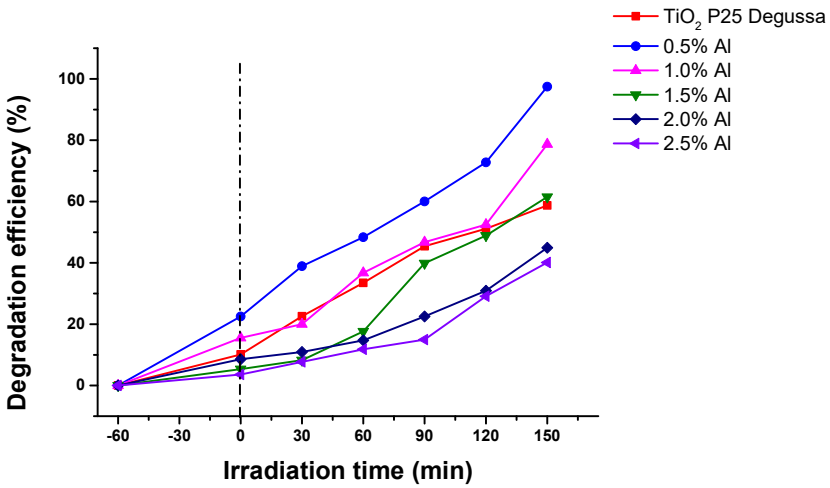

Figure 9. Photocatalytic degradation of Allura Red by Al – TiO_2 nanostructures.

As can be seen in Figure 9, 97.46% of Allura Red was photodegraded in the presence of 0.5 Al sample after 150 min, i. e. 1.65% times higher than commercial TiO_2 P25 Degussa. The Degradation efficiency of all the samples are presented in Table 3.

The photocatalytic process can be evaluated by the Langmuir –Hinselwood expression: $-ln\left(\frac{C_t}{C_o}\right) = kt$,, unde C_0 and C_t are the dye concentration at time 0 and t (after irradiation), k (min-1) is the pseudo - first order rate constant. The calculated rate constants and correlation coefficients

Preprints (www.preprints.org) | NOT PEER-REVIEWED | Posted: 4 December 2023 doi:10.20944/preprints202312.0192.v1

corresponding to Figure 10 are presented in Table 3. The acquired k values suggest that the best performance was obtained using 0.5% Al.

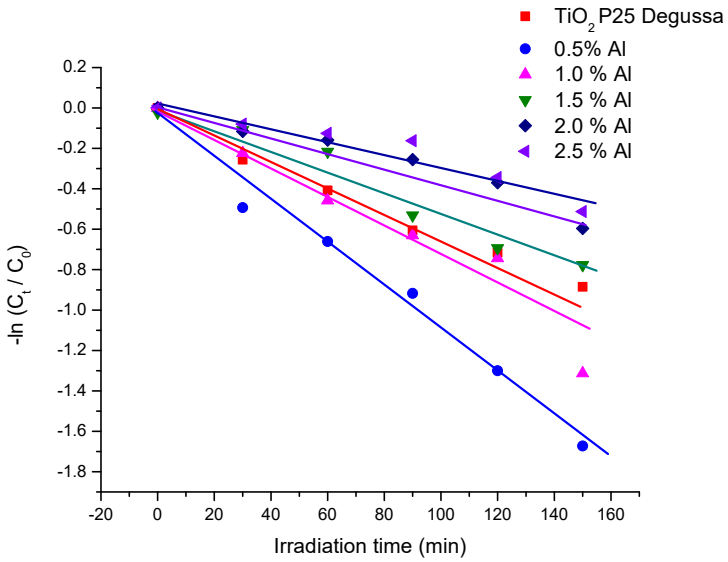

Figure 10. Kinetics of Allura Red degradation.

The calculated rate constants and correlation coefficients corresponding to Figure 10 are presented in Table 3. As can be see, 97.46% of Allura Red was photodegraded after 150 min, i. e. 1.65% times higher than commercial TiO_2 Degussa P25. The acquired k values suggest that the best performance was obtained using 0.5% Al.

Habibpanah et al. [43] reported also the reduction in titania photocatalytic activity due to increasing oxygen deficiency, which induce a faster rate of electron – hole recombination and leads to a reduced photocatalytic activity.

Table 3. Photodegradation rate, apparent first-order rate constant (k_i) of photocatalytic degradation and correlation coefficient (R^2).

Sample	Photodegradation rate (%)	$k_i \cdot 10^{-3}$	R^2
TiO_2 Degussa P25	58.72	3.21	0.98442
0.5% Al	97.46	9.70	0.98782
1.0% Al	73.66	5.78	9.95895
1.5% Al	61.51	6.29	0.92502
2.0% Al	44.91	4.44	0.93028
2.5% Al	40.11	4.94	0.89307

Scavanger experiments

To carry out this experiment, scavengers were added to the test solution under optimal conditions obtained as previous was descripted.

Figure 11 shows the addition of vitamin C for O_2^- and tert butanol for OH^-, act as a scavengers exhibit photodegradation efficiency within 150 min. the percentage of Allura Red degradation after 150 min in the presence of vitamin C was 7.46%, and for tert-butanol was 4.06% (Figure 11), demonstrating the relevance of hydroxyl and single oxygen radicals to Allura Red.

Preprints (www.preprints.org) | NOT PEER-REVIEWED | Posted: 4 December 2023 doi:10.20944/preprints202312.0192.v1

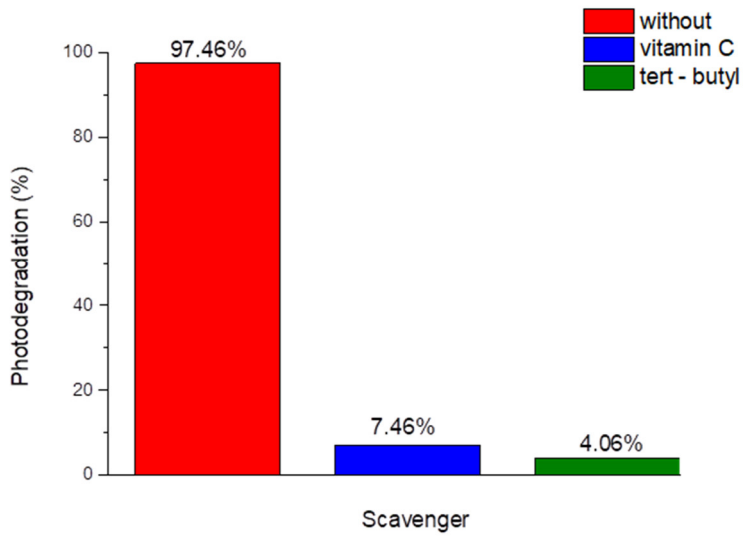

Figure 11. Photocatalytic degradation of Allura Red solution containing scavengers.

Effect of the solution pH on pollutant eliminations

The acidity and basicity of the wastewater produced by industrial entities has an important role during heterogeneous photocatalysis since it affects the surface of TiO_2 and the charge of substrates [44]. To examine the influence of pH value, NaOH and HCl were used to adjust de activity of the Allura Red – dispersed solution. Figure 12 indicates the photocatalytic degradation of Al – TiO_2 nanostructure at different initial pH value of 2, 6 and 11 under UV irradiation as a function of test time.

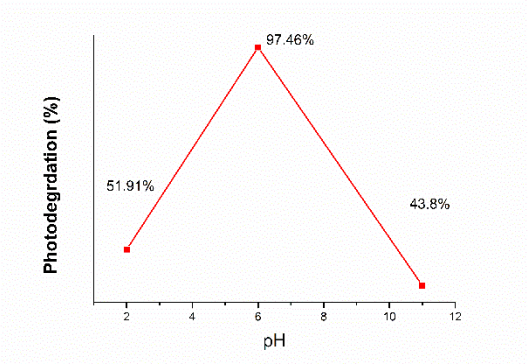

Figure 12. Effect of initial solution pH on Allura Red.

Photocatalytic cycling experiments

To evaluate the stability and reusability of the Al modified TiO_2 based nanoparticles photocatalyst in Allura Red dye, the recycling experiments were carrier out for 3 runs. After each cycle the recovered photocatalyst was separated from the solution, and after washing several times with deionized water and dried, and reused in the degradation for the next time. As show in Figure 13. the photodegradation efficiency reduced from 97.46% to 93.93%. The main reason behind this descending trend is the weight loss of the photocatalytic during the each run. This fact indicates that the samples still maintain a relatively high photodegradation capacity and good reusability after 3 runs under visible light irradiation and constant experimental conditions. The Allura Red dye degradation efficiency is well – preserved above 96.93%, as mentioned, even three cycles, indicating excellent stability of the photocatalyst in the degradation of Allura Red.

Preprints (www.preprints.org) | NOT PEER-REVIEWED | Posted: 4 December 2023 doi:10.20944/preprints202312.0192.v1

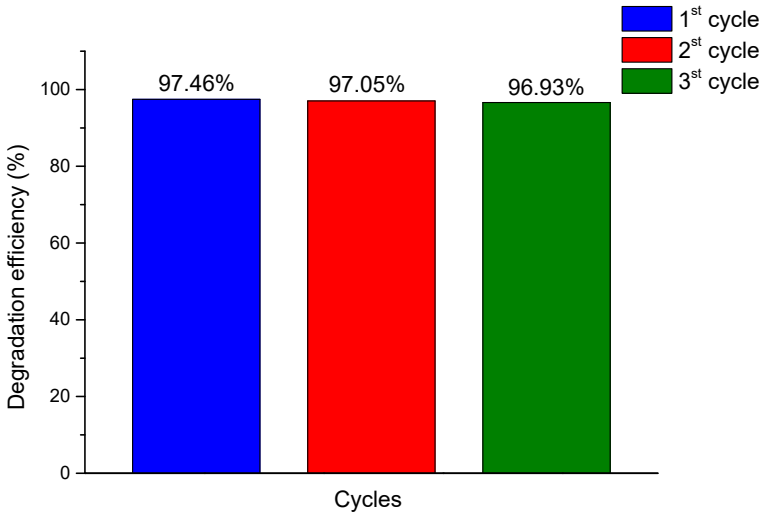

Figure 13. The reusability of Al doped titania for degradation of Allura Red.

Photocatalytic mechanism. Reactiv Oxigen Species (ROS) Generation

To identify the reactive species generated by 0.5%Al sample, EPR coupled with spin trapping technique was used. After 25 min of irradiation with UV light a complex spectrum was obtained. To separate contribution of generated ROS, a simulation of the spectrum was performed. The best simulation contain a linear combination of the following spin adducts: •DMPO–CH_3 (aN = 13.2 G, aH = 8.2 G, , aH = 1.8 G, g = 2.0098 relative concentration 58%), •DMPO–O^{2-} (aN = 12.7 G, aH = 10.2, aH = 0.8 G, g = 2.0098, relative concentration 19%), and nitroxide-like radical (aN = 13.6 G, g = 2.0098, relative concentration 23%). The •DMPO–CH_3 adduct is form by the interaction between the produced •OH radical and the DMSO solvent. Consequently, the sample generates both •OH and •O^{2-} radicals, the main species being •OH.

The other specie observed is the nitroxide radical resulted by cleavage of the N-C bond and ring opening of DMPO [45].

3. Materials and Methods

3.1. Materials and sample preparation

This novel method can be divided in two basic steps: (i) obtaining of aluminium waste from end – of – life vehicles, (ii) pure and TiO_2 modified materials preparation.

3.1.1. Aluminium waste from end – of – life vehicle

The shredding phase was obtained, after car collecting and dismantling, using the Shredding installation, Lindemann mark.

The shredder installation is specifically for the processing of large metal waste, parts, and sub-assemblies from end-of-life vehicles. For testing, the shredded phase resulting from the chopping plant was used with average dimensions of 3x4 mm in cross section and 50-60 mm in length.

The preparation of the crushed phase consisted of the removal of foreign bodies and their compactation using a manual press. Molds of easy-to-handle material with a small specific surface were obtained, to avoid losses through oxidation.

The melting of the aluminum waste thus prepared was carried out in a flame furnance, with a crucible of 3 kg capacity. The time of a processing batch to obtain recycled aluminum were 2.5 h. To avoid contamination of the liquid alloy bath with oxides and gases from the environment were used specific covering materials. The slag formed during melting was removed twice: the first time when the melt was completely formed and the last time before exiting the furnance, for an alloy as clean as possible. The aluminum alloy was cast at a temperature of 720 °C, in molds from the forming mixture

 doi:10.20944/preprints202312.0192.v1

resulting in simple parallelepiped samples 20x22 mm and 300 mm long. The cast and cooled samples were debited and prepared for machining.

Aluminum powder was obtained by cold machining process of the sample on a universal milling machine.

3.1.2. Preparation of Al – TiO_2 nanoparticle.

The TiO_2 based materials were produced by solide state reaction. As starting chemical were used: P25 TiO_2 commercial powder (Degussa AG, Germany), acetylacetone (Merck, Germany) and Tween 80 (Merck, Germany). Titania nanopowder (5g) was dispersed into 10ml deionized water, adding then 1.2 ml mixture of acetylacetone : Tween 80 (1:2 volumetric ratio) in order to obtain a better dispersion and particle uniformity and Al waste in the ration of n(Ti) / n(Al) = x (x = 0.0; 0.5; 1.0; 1.5; 2.0 and 2.5). The homogenous obtained by mixing the reagents with a magnetic stirrer is keeped 5 days at 20° and the is sintered using a conventional furnance at 500°C, 2h, with a temperature ramp of 10°C/min.

3.2. Characterization

Thermal analysis (TG–DTA–DTG) was recorded with a Mettler-Toledo Thermogravimeter 851e equipment. The TG–DTA–DTG was performed in air, in the temperature range 20–1000°C using upgraded computer controlled equipment. About 38,679 mg of sample was heated in Pt-holder with another Pt-holder containing a-alumina as reference material. The sample was heated at a rate of 10°C/min from ambient temperature to 1000°C in static air.

The XRD was recorded on the BRUKER D8 Advance X-ray diffractometer, working at 45kV and 45mA. The CuKα radiation, Ni filtered was collimated with Soller slits. A germanium monochromator was used. The data of the X-ray diffraction patterns were collected in a step-scanning mode with steps of $\Delta 2\theta = 0.01°$. Pure silicon powder (standard sample) was used to correct the data for instrumental broadening. The Warren - Averbach X-ray profile Fourier analysis of the (101), (004) (200) and (204) anatase peak profiles were processed by the XRLINE [20] computer program in order to determine the effective crystallite mean size (D_{eff}). The crystallite size distribution function was determined from the second derivative of the strain corrected Fourier coefficients [21]. FT-IR spectra of the powder samples using KBr pellet technique, in the absorbance mode have been recorded using JASCO FT/IR-6100 Fourier Transform Infrared Spectrometer in the 400 - 4000cm^{-1} wavenumber range with a resolution of 2cm^{-1}.

For the morphology of samples, a Scanning Electron Microscope Hitachi SU8230 scanning electronic microscope (Tokyo, Japan), using 30 kV, 15 mm working distance. The instrumental analysis of the sample composition was determined by Oxford Instruments EDS System (Oxford, UK) and AZtech software (Greeley, CO, USA).

Optical UV–VIS absorption spectra were recorded on the PERKIN-ELMER LAMBDA 45 spectrophotometer (JASCO International Co., Ltd., Tokyo, Japan), equipped with an integrating sphere assembly of 200–900 nm. This characterisation method was used to determine the band gap energy of the Al – TiO_2 samples and to know its relationship with the amount of Al used. The band gap was estimated from the Tauc's equation.

Photocatalytic measurements were performed by immersing the 0.5 mg samples in the Allura Red solution ($c_o = 2 \times 10^{-5}$) irradiated with UV lamp (15 W) emitting at 365 nm.

The absorbance of the Allura Red solution was measured using a T80+ UV–VIS, Pro Instruments Ltd. Spectrophotometer (Leicestershire, UK). The effect of the initial 2–11 pH solution on the degradation of Allura Red, under a UV lamp (15 W) emitting at 365 nm for 150 min was also determined.

5,5-dimethyl-1-pyrroline N-oxide (DMPO, Sigma-Aldrich, Merck, KGaA, Darmstadt, Germany) was used as a spin-trapping reagent. The nanoparticles (10 mg) were dispersed in DMSO (1 mL) and homogenized in an ultrasound bath (30 min) before use. DMPO of 0.2 mol/ concentration was added to the suspension. The samples were prepared immediately before measurements and transferred into the quartz flat cell optimized for liquid measurements.

5. Conclusions

Aluminium scrap from end – of – life vehicles modified TiO_2 nanoparticle was succesfully synthesized by solid state reaction and its capability to photodegrade the Allura Red dye was evaluated in different conditions in therms of pH value, in presence of scavengers and the recycling experiments for 3 runs.

XRD calculations also showed that the a and c parameter of TiO_2 anatase change slightly, as results the cell volume changes. The opto-electronic properties shows that Al addition shifted the absorption spectra toward the visible range. The highest photocatalytic activity (79.99%) was achieved for the sample containing 0.5% Ag. A higher concentration of Al particles shields the active centers of the semiconductor, thus reducing its catalytic activity. The Langmuir – Hinselwood kinetic model can be efficiently applied for describing the Allura Red photodegradation under UV irradiation. The •OH are the main species generated and responsible for Allura Red degradation.

Author Contributions: Conceptualization, R.-C.S. and S.E.A.; investigation, R.-C.S., M.S., A.P., D.T., A.M., C.V. and C.T.; methodology, R.-C.S., S.E.A. and A.M.; writing—original draft, R.-C.S., S.E.A. and D.T.; writing—review and editing, R.-C.S., S.E.A., A.P., A.M. and D.T. All authors have read and agreed to the published version of the manuscript.

Funding: This research was funded by the MCID through the "Nucleu" Program within the National Plan for Research, Development, and Innovation 2022–2027, project PN 23 24 01 03 and by a grant of the Romanian Ministry of Education and Research. CNCS-UEFISCDI, project PN-III-P1-1.1-TE-2021-0661 and PN-III-P1-1.1-TE-2021-0358 within PNCDI III

Conflicts of Interest: The authors declare no conflict of interest.

References

1. Samal, P., Vundavilli, P. R., Meher, A., Mahapatra, M. M. Recent progress in aluminum metal matrix composites: A review on processing, mechanical and wear properties. *J Manuf Process* **2020,** 59, 131-152 doi:10.1016/j.jmapro.2020.09.010
2. Salman, K. D., Al – Maliki, W. A. K., Alobaid, F., Epple, B. Microstructural analysis and mechanical properties of a hybrid Al / Fe_2O_3 / Ag nano-composite. *Appl Sci* **2022** 12, 730 doi: 10.3390/app12094730
3. Billy, R. G., Müller, D. B., Aluminum use in passenger cars poses systemic challenges for recycling and GHG emissions. *Resour Consserv Recycl* **2023,** 190, 106827 doi: 10.1016/j.resconrec.2022.106827
4. Ingaldi, M., Borkowski, S., Recycling process of the aluminium cans as an element of the sustainable development concept. *Manuf Technol* **2014,** 14 (2), 172-178 doi: 10.21062/ujep/x.2014/a/1213-2489/MT/14/2/172
5. Shinzato, M. C., Hypolito, R. Solid waste of aluminium recycling process: characterization and reuse of its valuable constituents, *Waste Manage* **2005,** 25, 37-46 doi: 10.1016/j.wasman.2004.08.005
6. Pamata, S. K., Yasinskiy, A., Polyakov. P. A review of secondary aluminium production and its byproducts. *JOM* **2021,** 73 (9), 2603-2614 doi:10.1007/s11837-021-04802-y
7. Jafari, N. H., Tark, T. D., Roper, R. Classification and reactivity of secondary aluminium production waste. *J Hazard Toxic Radioact Waste* 2013, 18 (4) 04014018 doi: 10.1061/(ASCE)HZ.2153-5515.0000223
8. [1] Capuzzi, S., Timelli, G. Preparation and melting of scrap in aluminium recycling: A review. *Metals* **2018,** 8 (4), 249-258 doi: 10.3390/met8040249
9. Bulei, C. Tudor, M. P., Kiss, I. Aluminium matrix composites- on overview on the materials substitution and efficient use of materials. *Acta Tehnica Corvininesis – Bull Eng* **2019,** 87 (2), 91-94
10. Billy, R. G., Müller, D. B., Aluminum use in passenger cars poses systemic challenges for recycling and GHG emissions. *Resour Consserv Recycl,* **2023,** 190, 106827 doi: 10.1016/j.resconrec.2022.106827
11. Ingaldi, M., Borkowski, S., Recycling process of the aluminium cans as an element of the sustainable development concept. *Manuf Technol* **2014,** 14 (2), 172-178 doi: 10.21062/ujep/x.2014/a/1213-2489/MT/14/2/172
12. Shinzato, M. C., Hypolito, R. Solid waste of aluminium recycling process: characterization and reuse of its valuable constituents, *Waste Manage* **2005,** 25, 37-46 doi: 10.1016/j.wasman.2004.08.005
13. Pamata, S. K., Yasinskiy, A., Polyakov. P. A review of secondary aluminium production and its byproducts. *JOM* **2021,** 73 (9), 2603-2614 doi:10.1007/s11837-021-04802-y
14. [1] Jafari, N. H., Tark, T. D., Roper, R. Classification and reactivity of secondary aluminium production waste. *J Hazard Toxic Radioact Waste* **2013**, 18 (4) 04014018 doi: 10.1061/(ASCE)HZ.2153-5515.0000223
15. Capuzzi, S., Timelli, G. Preparation and melting of scrap in aluminium recycling: A review. *Metals* **2018,** 8 (4), 249-258 doi: 10.3390/met8040249

16. Bulei, C. Tudor, M. P., Kiss, I. Aluminium matrix composites- on overview on the materials substitution and efficient use of materials. *Acta Tehnica Corvininesis – Bull Eng* **2019,** 87 (2), 91-94
17. Prosviryakov, A., Bazlov, A.The study of thermal stability of mechanically alloyed Al – 5wt% TiO_2 composites with Cu and stearic additives. *Appl Sci* **2013,** 13, 1104 doi:10.3390/app13021104
18. Liu, J., Xu, M., Zhang, T., Chu, X., Shi, K., Li, J. Al / TiO_2 composite as a photocatalyst for the degradation of organic pollaunts. *Environ Sci Pollut Res* **2023,** 30, 9738 – 9748 doi:10.1007/s11356-022-22861-9
19. Lee, D. Y., Lee, M. – H., Lim, B. – Y.. Cho, N. – I. Crystal structure and photocatalytic activity of Al – doped TiO_2 nanofibers for methylene blue dye degradation, *J Nanosci Nanotechnol* **2016,** 16 (5), 5341-5344 doi:10.1166/jnn.2016.12273
20. Aldea, N., Indrea, E. Xrline, a program to evaluate the crystallite size of supported metal-catalysts by single X-ray profile fourier-analysis. *Comput Phys Commun* **1990,** 60, 155-159 doi: 10.1016/0010-4655(90)90084-E
21. Indrea, E., Barbu, A. Indirect photon interaction in PbS photodetectors. *Appl Surf Sci,* **1996,** 106, 498 doi:10.1016/S0169-4332(96)00394-7
22. van Berkum, J. G. M., Vermeulen, A. C., Delhez, R., de Keijser, T. H., Mittemeijer, E. M. Applicabilities of the Warren-Averbach analysis and an alternative analysis for separation of size and strain broadening. *J Appl Cryst* 1994, 27, 345 – 357 doi: 10.1107/S0021889893010568
23. Kraus, W., Nolze, G. POWDER CELL — a Program for the representation and manipulation of crystal structures and calculation of the resulting X-ray powder patterns, *Appl Cryst* **1996**, 29, 301—309 doi: 10.1107/S0021889895014920
24. de los Santos. D. M.; Aguilar, T.; Sánchez – Coronilla, A.; Navas, J.; Hernández, N. C.; Alcántara, R.; Fernáandez – Lorenzo, C.; Martín – Calleja, J. Electronic and Structural properties of highly aluminium ion doped TiO_2 nanoparticles: a combined experimental and theotetical study, *Chem Phys Chem* 214, 15, 2267
25. Khlyustova, A.; Sirotkin, N.; Kuova, T.; Kraev, A.; Titov, V.; Agafonov, A. Doped TiO_2: the effect of doping elements on photocatalytic activity. *Mater Adv,* **2020**, 1, 1193-1201 doi:10.1039/D0MA00171F
26. Kaewsaenee, J.; Visal – athaphand, P.; Supaphol, P.; Pavarajarn, V. Fabrication and charcterization of neat and aluminum – doped titanium (IV) oxide fibers prepared by combined sol – gel and electrospinning techniques. *Ceram Int* **2010**, 36 (7) 2055 -2061
27. Alsulami, Q. A. Arshad, Z., Ali, M. Wageh, S. Efficient tuning of the opto-electronic properties of sol–gel-synthesized Al-doped titania nanoparticles for perovskite solar cells and functional textiles. *Gels* **2023,** 9, 101 doi: 10.3390/gels9020101
28. Khalil, M. Medhat, M., Elshaer, A. M., Soliman, M. Ebrahim, S., Khali, M. Aluminium oxide nanoparticles as a photocatalyst for water splitting, Preprint (2022) doi:10.21203/rs.3.rs-1323825/v1
29. Hubert Joe, I., Vasudevan, A. K., Aruldhas, G. ,Damodaran, A. S., Warrier, K. G. K. , FTIR as a tool to study high-temperature phase formation in sol–gel aluminium titanate. *J Solid State Chem* 1997, 13 (1), 181 – 184 doi:10.1006/jssc.1997.7371
30. Choi, W., Termin, A. , Hoffmann, M. R., The role of metal ion dopants in quantum-sized TiO_2: correlation between photoreactivity and charge carrier recombination dynamics, *J Phys Chem* **1994,** 98, (51), 13669 - 13679 doi:10.1021/j100102a038
31. Chalasani, R., Vasudevan S. Cyclodextrin-functionalized Fe_3O_4@TiO_2: reusable, magnetic nanoparticles for photocatalytic degradation of endocrine-disrupting chemicals in water supplies. *ACS Nano,* **2013,** 7 (6), 4093 – 4104 doi: 10.1021/nn400287k
32. Liu, S., Liu, G., Feng, Q. Al – doped TiO_2 mesoporous materials: synthesis and photodegradation properties. *J Porous Mater* **2010**, 17, 197 - 206 doi: 10.1007/s10934-009-9281-8
33. Fujishima, A., Rao, T. N., Tryk, D. A. Titanium dioxide photocatalysis, *J Photochem Photobiol C* **2000,** 1(1), 1 - 21 doi:10.1016/S1389-5567(00)00002-2
34. Liu, J., Xu, M., Zhang, T., Chu, X., Shi, K. Li, J. Al/TiO_2 composite as a photocatalyst for the degradation of organic pollutants, *Environ Sci Pollut Res* **2023**, 30, 9738–9748 doi: 10.1007/s11356-022-22861-9
35. Kumar, S., Verma, N. K., Singla, M. L. Study on reflectivity and photostability of Al – doped TiO_2 nanoparticles and their reflectors. *J Mater Res,* **2013,** 28, 521-528 doi: 10.1557/jmr.2012.361
36. Shaitanova, L., Murashkinab, A., Rudakovaa, A., Ryabchuka, V., Emelinea, A., Artemevb, Y., Kataevac, G., Serponed, N. UV-induced formation of color centers in dispersed TiO_2 particles: Effect of thermal treatment, metal (Al) doping, and adsorption of molecules, *J Photochem Photobiol A* **2018,** 54, 33–46 doi:10.1016/j.jphotochem.2017.07.038 1010-6030
37. Ray, H. The independence of scattering length on van de Waals interaction and reduced mass of the system in two-atomic collision at cold energies. *Pramana* **2016,** 87 (1), 8 doi: 10.1007/s12043-016-1221-y
38. Azarniya, A. Soltaninejad, M., Zekavat, M., Bakhshandeh, F., Hosseini, H. R. M., Amutha, C., Ramakrishna, Application of nanostructured aluminiujm titanatwe (Al2TiO5) photocatalyst for removal of irganic pollunants from water: Influencing factors and kinety study. *Mat Chem* Phys **2020**, 256, 123740doi:10.1016/j.matchemphys.2020.123740
39. Klalid, N. R. Liaqar, Tahir, M. M. B., Nabi. G., Iqbal, T., Niaz, N. A. The role of grafene and europium dperformance for photocatalytic hydrogen evolution. *Ceram Int* **2018,** 44, 546-549 doi: 10.1016/j.ceramint.2017.09.209

40. M. Masoudi, M. Mashreghi, E. Goharshadi, A. Meshkini, Multifunctional fluorescent titania nanoparticles: green preparation and applications as antibacterial and cancer theranostic agents. *Artif Cell Nanomed Biotechnol* **2018,** 46 (2), 248-259 doi: 10.1080/21691401.2018.1454932
41. Tripathi, A. K. Mathpal, M. C. Thakur, P. Agrahari, V., Singh, M. K., Mishra, S. K. Ahmad, M. M, Agarwar, A. Photoluminescence and photoconductivity of Ni doped titania Nanopartcicles. *Adv Mat Lett* **2015**, 6 (3), 201 – 208 doi: 10.5185/amlett.2015.5663
42. Hema, M., Yelil Arasia, A., Tamilselvia, P., Anbarasan, R. Titania nanoparticles synthesized by sol-gel technique. *Chem Sci Trans,* **2013,** 2 (1) 239-245 doi: 10.7598/cst2013.344
43. Habibpanah, A. A., Pourhashem, S., Sarpoolaky, H. Preparation and characterization of photocatalytic titania–alumina composite membranes by sol–gel methods. *J Eur Ceram Soc* **2011,** *31,* 2867–2875 doi: 10.1016/j.jeurceramsoc.2011.06.014
44. Bouanimba, N., Laid, N., Zouaghi, R., Sehili, T. Effect of pH and inorganic salts on the photocatalytic decolorization of methyl orange in the preserved of TiO_2 P25 and PC250, *Desalin Water Treat* **2015,** 53, 951-963 doi: 10.1080/19443994.2013.848667
45. Bosnjakovic A., Schlick, S. Spin trapping by 5,5 – dimethylpyrroline-N-oxide in Fenton media in the presence of Nafion perfluorinated membranes: limitation and potential. *J Phys Chem B* 2006, 110, 10720-10728, doi: 10.1021/jp061042y